Journal of Structural Geology 118 (2019) 236–249

Contents lists available at ScienceDirect

Journal of Structural Geology

journal homepage: www.elsevier.com/locate/jsg

Structural controls on the interaction between basin fluids and a rift flank fault: Constraints from the Bwamba Fault, East African Rift

Allan D. Hollinsworth[a,*], Daniel Koehn[a], Tim J. Dempster[a], Kevin Aanyu[b]

[a] School of Geographical and Earth Sciences, Gregory Building, University of Glasgow, Glasgow G12 8QQ, UK
[b] Department of Geology and Petroleum Studies, University of Makerere, Wandegeya, Makerere, P.O. Box 7062, Kampala, Uganda

ARTICLE INFO

Keywords:
Faults
East African Rift
Permeability evolution
Fluid-rock interaction
Mineralisation
Hydrogeology

ABSTRACT

We present petrographic and structural analyses of a basement-hosted border fault in the East African Rift. Understanding the mechanical evolution and fluid-rock interaction of rift-flank faults is integral to developing models of fluid flow in the crust, where hydraulic connections may occur between basement faults and basin sediments. The Bwamba Fault forms the flank of the Rwenzori Mountains Horst in western Uganda, and has locally reactivated older mylonitic fabrics in the basement gneisses. The fault core features discrete mineralised and veined units. Shear fabrics and fault scarp striations indicate predominately normal kinematics, with minor strike-slip faulting and fabrics. Transient brittle failure was accompanied by two phases of fluid ingress, associated with veining and mineralisation. The first was localised and strongly influenced by host lithology. The second involved widespread Fe-oxide and jarosite mineralisation. The latter signals the onset of a hydraulic connection between Fe- and S-rich sedimentary rocks in the adjacent Semliki Rift Basin and the Bwamba Fault, involving co-seismic and or post-seismic fluid injection into the fault at ca. 150–200 °C, and 2.5–3 km depth. Such evolving permeability connections between basin sediments and basement faults are important for local hydrocarbon and geothermal systems, and may be typical of active rifts.

1. Introduction

1.1. Fault zones and fluid flow

Fault zones localise strain and modify the porosity and permeability of crustal lithologies at a range of scales. Heterogeneous, anisotropic permeability networks are developed in fault zones hosted in impermeable crystalline basement rocks. Such networks evolve with the creation of new pathways, fluid-enhanced mineral replacement reactions (Lawther et al., 2016), and reactivation of existing fabrics (Salomon et al., 2015; Hodge et al., 2018). Developing models for the evolution of basement fault architecture and hydrology is central to understanding crustal fluid flow, particularly in rift settings where basement-hosted faults progressively interact with hanging wall rift-basin sediments (Lueth et al., 2005; Hollis et al., 2017; Kristensen et al., 2016).

The basis for understanding the hydraulic properties and structure of fault zones stems from the work of Caine et al. (1996). The lithology and structural characteristics of the protolith has an important role in many fault systems. Granite, gneisses and granitic mylonites, have low permeability, with variations linked to porosity and confining pressure (Wibberley and Shimamoto, 2002). Once a fault system has been established, the hydraulic properties of the crust become controlled by fault rocks, fabrics and mineralisation in the fault core, and fracture fabrics in the damage zone (Caine et al., 1996; Mitchell and Faulkner, 2012). Damage zones in low permeability host rocks are typically important for fluid migration, and commonly show evidence of veining and chemical alteration (Wibberley and Shimamoto, 2002; Lawther et al., 2016; Kristensen et al., 2016). Changes in deformation mechanisms (Zhu and Wong, 1997), veining, and mineralisation (Holdsworth et al., 2011) may modify fault zone permeability of fault rocks. Equally important is the temporal change to permeability generated by the earthquake cycle (Sibson, 1990). Several fault zones show evidence of having experienced transient pulses of high fluid flux caused by fluid overpressure induced seismicity (Sibson, 1990; Cox, 1995; Japas et al., 2016), This process is not well established for normal fault systems (Sibson, 2000) or in fault zones within shallower parts of the upper crust (Japas et al., 2016) where coupling between basin and fault zone hydrological systems may occur (Hollis et al., 2017). There is therefore a need to develop a more robust understanding of shallow

* Corresponding author.
E-mail addresses: a.hollinsworth.1@research.ac.uk (A.D. Hollinsworth), daniel.koehn@glasgow.ac.uk (D. Koehn), tim.dempster@glasgow.ac.uk (T.J. Dempster), kaanyu@cns.mak.ac.ug (K. Aanyu).

https://doi.org/10.1016/j.jsg.2018.10.012
Received 30 March 2018; Received in revised form 2 October 2018; Accepted 15 October 2018
Available online 01 November 2018

crustal fault zone processes, as these depths coincide with active seismicity (Lindenfeld et al., 2012), groundwater and geothermal (Ochmann et al., 2010), and hydrocarbon systems (Trice, 2014).

Here, we present petrographic and structural analyses of fluid-rock interaction at shallow crustal levels in the Bwamba Fault Zone (BFZ), western Uganda, with the aim of characterising the dynamic permeability and hydraulic properties of an upper crustal fault zone hosted in low permeability, granitic host rock. We discuss the mechanical and hydrological evolution of the basement-hosted BFZ, and its hydrodynamic relationship with sedimentary rocks and formation fluids in the Semliki Basin, with implications for the behaviour of subsurface fluid systems in the western branch of the East African Rift System.

1.2. Geological setting

1.2.1. The East African Rift System

The Bwamba Fault is a major rift flank fault in the western branch of the 4000 km long East African Rift System (EARS), separating the sediments of the Semliki Basin from uplifted basement rocks of the Rwenzori Mountains. The EARS is composed of two axial rift branches (east and west), each characterised by en-echelon axial rift basins (Ebinger, 1989; Upcott et al., 1996, Fig. 1.). The onset of significant rifting processes occurred at ~30 Ma for both the eastern (Hofmann et al., 1997) and western (Roberts et al., 2012) rift segments of the EARS. Along the western branch of the EARS, crustal thicknesses range between 36 and 44 km beneath the Tanzania Craton (Fig. 1a) and surrounding mobile belts (Last et al., 1997). The crust beneath the eastern Albert rift shoulder is 30 km thick, and varies between 20 and 28 km beneath the Rwenzori Mountains to the south (Wölbern et al., 2010).

1.2.2. The Albertine Rift System

The Albertine Rift System (Fig. 1a) is formed of the Albert, Semliki, George, and Edward rift basins, and is the northernmost segment of the western branch of the EARS (Ebinger, 1989, Fig. 1). The Albert Basin (Fig. 1a) forms a symmetric graben and contains 5–6 km of Miocene to Holocene fluvial, deltaic and lacustrine sedimentary rocks with several hydrocarbon plays (Upcott et al., 1996; Logan et al., 2009; Roller et al., 2010). At the northern end of the Rwenzori Mountains (Fig. 1), the thickness of the Albert Basin sediments decreases to ~600 m (Roller et al., 2010). On its SW margin, the Albert Basin terminates against a north-east trending faulted monocline that forms the northern boundary of the Semliki Basin (Upcott et al., 1996).

The Semliki Basin extends ~150 km from its northern boundary with the Albert Basin to a narrow termination with the Edward Basin (Fig. 1b), its axis changes from NE-SW in its northern half to N-S in its southern half. The steeply WNW/NW-dipping Bwamba Fault forms its eastern boundary (Fig. 1 b–d), whilst the Semliki Fault marks its western limit (Fig. 1). Seismic surveys from the north of the basin indicate that depths to basement vary between 3 and 6 km (Kiconco, 2005, Fig. 1d). Syn-rift extensional and post-rift compressional faults have been identified from seismic surveys in the Semliki rift; additionally, a prominent flower structure in a transfer zone along the NE margin of the rift that affects basement and cover rocks has also been identified, indicative of syn-rift strike slip tectonics (Kiconco, 2005). The Semliki Basin is filled by similar fluvio-deltaic and lacustrine sedimentary rocks to the Albert Basin, with the latter dominated by diatomite and bivalve-bearing mudstones, evaporites and sandstones, whilst the fluvio-deltaic periods are characterised by channelised sandstones (Kiconco, 2005). The recent uplift of the Rwenzori rift shoulders from ~2.5 Ma (Schneider et al., 2016) resulted in a change of sediment supply to produce a more proximal coarse-grained alluvium (Kiconco, 2005).

1.2.3. The Rwenzori Mountains

The Rwenzori Mountains form a horst block located in a rift transfer zone in the ARS, bordered by the Semliki rift to the west, and the actively propagating Albert and George rifts to the east (Koehn et al., 2010 (Fig. 1b). The horst exhibits anomalous topography for its extensional tectonic setting (over 5000 m) facilitated by uplift along its steep, high relief western flank, well-defined by the Bwamba Fault, with a lower relief eastern flank still partially attached to the Tanzania craton (Koehn et al., 2010; Bauer et al., 2012). A NNE-SSW narrow (7–16 km wide), lower elevation (1000–3400 m) ridge defines the northern end of the Rwenzori block (Fig. 1c). To the south, a wider (≤50 km), higher elevation (1000–5000 m) glaciated massif is present (Bauer et al., 2012).

The Rwenzori horst is composed of a suite of banded granitic and amphibolitic gneisses and paragneisses (Fig. 1b), correlated with the 2.6 Ga Aruan Group of the Ugandan basement complex (Link et al., 2010). The gneisses have experienced polyphase deformation within a Palaeoproterozoic orogenic belt, along with the metasedimentary and metavolcanic rocks of the Buganda-Toro belt (Fig. 1b) (Link et al., 2010). Contacts between the basement gneisses and metasediments and metavolcanics are marked by mylonites (Link et al., 2010). Thermochronological (Bauer et al., 2010) and sedimentological data indicates the Rwenzori horst has experienced 3 km of uplift above general ~2 km elevations of rift shoulders in the Albertine Rift System within the last ~2.5 Myr. Several uplift mechanisms have been proposed for the block. The presence of a strong lithosphere with a high elastic thickness due to the presence of amphibolites beneath the central Rwenzoris may enable the formation of deeper faults that facilitate more significant uplift than rifts nucleating in lower-strength crust with shallow-terminating faults (Sachau and Koehn, 2010). Active magmatism replacing cold, dense lithospheric cratonic material has also been suggested to contribute to the uplift of the Rwenzoris (Wallner and Schmeling, 2010), given the presence of low-velocity anomalies beneath the central Rwenzoris indicating thinned crust (Wölbern et al., 2010). Crucial to all mechanisms is the accommodation of strain on the Bwamba fault, which is estimated to have hosted ~10 km of displacement at its centre, adjacent to the Rwenzori massif (Ring, 2008). Displacement is thought to be less near the northern tip zone of the fault, at Sempaya (Fig. 1) where estimates of 6.9 km have been proposed (Ring, 2008).

2. Methods

Fieldwork was undertaken in western Uganda during September 2016. Structural measurements of the Bwamba Fault scarp, brittle fabrics and kinematic indicators, and samples of in-situ protolith, and cataclasite-series rocks from the fault core were collected. Samples were cut parallel to the dip-direction of the fault, and thin sections prepared for optical and SEM microscopy. Cut hand specimens were oriented to field-position using adhesive putty and rigid boards in order to measure structures not visible in the field. SEM and spectral analyses were undertaken at the ISAAC facility at the University of Glasgow, using a Carl Zeiss Sigma environmental SEM operated at 20 kV with Oxford Instruments X-Max 80 energy dispersive spectrometry and data processed with AZTEC software 3.0. Thin section scans were made using an Epson Perfection 4990 Photo Scanner in 24 bit-colour at resolutions of 1200 dpi. A Nikon XTH 320/225 microscope camera was used for photomicrographs.

3. Results

3.1. Field-scale observations of the Bwamba Fault Zone

The Bwamba Fault Zone (BFZ) is exposed between N 0°50′2.05″ E 30°10′8.86” (locality A) and N 0°49′41.12″ E 30°9′57.75” (locality C), ca. 500 m west of the Sempaya hot springs (Fig. 1). The exposure forms a high relief flank to the Semliki rift. The lower 20–30 m of the fault scarp is covered by dense rainforest, whilst the upper surfaces have less vegetation (Fig. 1). Three main exposures were studied along the length of the scarp (Fig. 1c); locality A is the northern-most exposure, locality

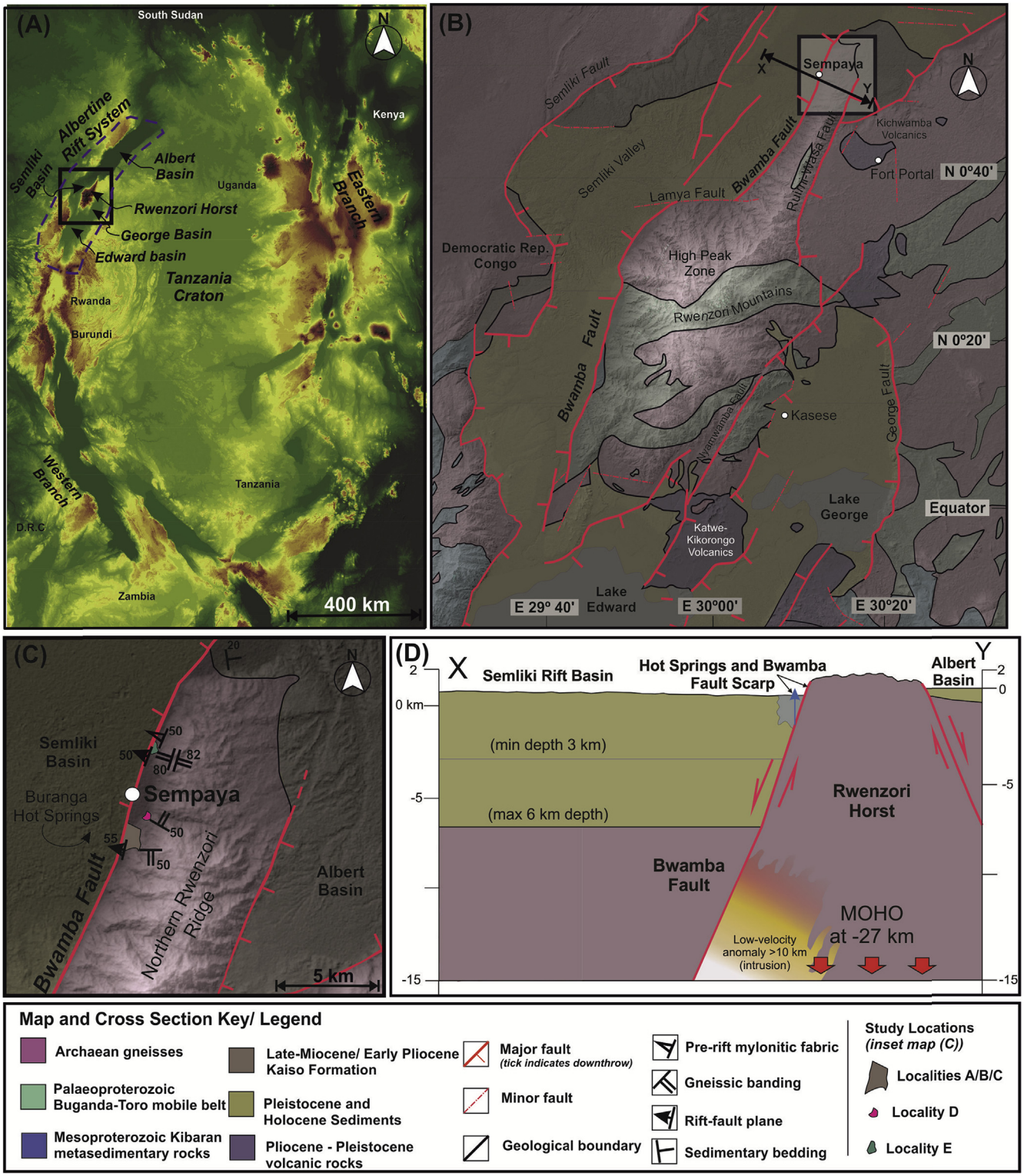

Fig. 1. a) 90 m Digital Elevation Model (DEM) of the central East African Rift System, showing the location of the east and west branches, the Albert, Edward, George, and Semliki Rift Basins that comprise the Albertine Rift System, and the Rwenzori Mountains in western Uganda; b) Geological map of the Rwenzori Mountains (after Ring (2008) and Koehn et al. (2010)), superimposed on a 30 m DEM; c) inset map showing study site, and measurement data acquired by the authors; d) Geological cross-section of X-Y line in (b); depths of the Semliki basin, and MOHO depths from Kiconco (2005) and Wölbern et al. (2010).

B (N 0°49′48.3″ E 30°10′3.6″ is an incised valley that reveals the fault core and part of the damage zone, and locality C is the southern-most exposure where the fault core is well exposed along a 20 m wide cliff face. Wall-rock lithologies and structural fabrics in the basement gneisses forming the protolith to the BFZ were studied at N 0°50′19.80″ E 30° 10′11.50” (locality D) and N 0°52′36.26″ E 30°10′40.06” (locality E). These locations are 0.5 and 4.77 km north of the fault zone where the basement rocks are exposed in small quarries. Due to the steep, forested terrain, the lateral extent of the footwall could not be established, whilst the hanging wall hosts sediments of the Semliki basin and

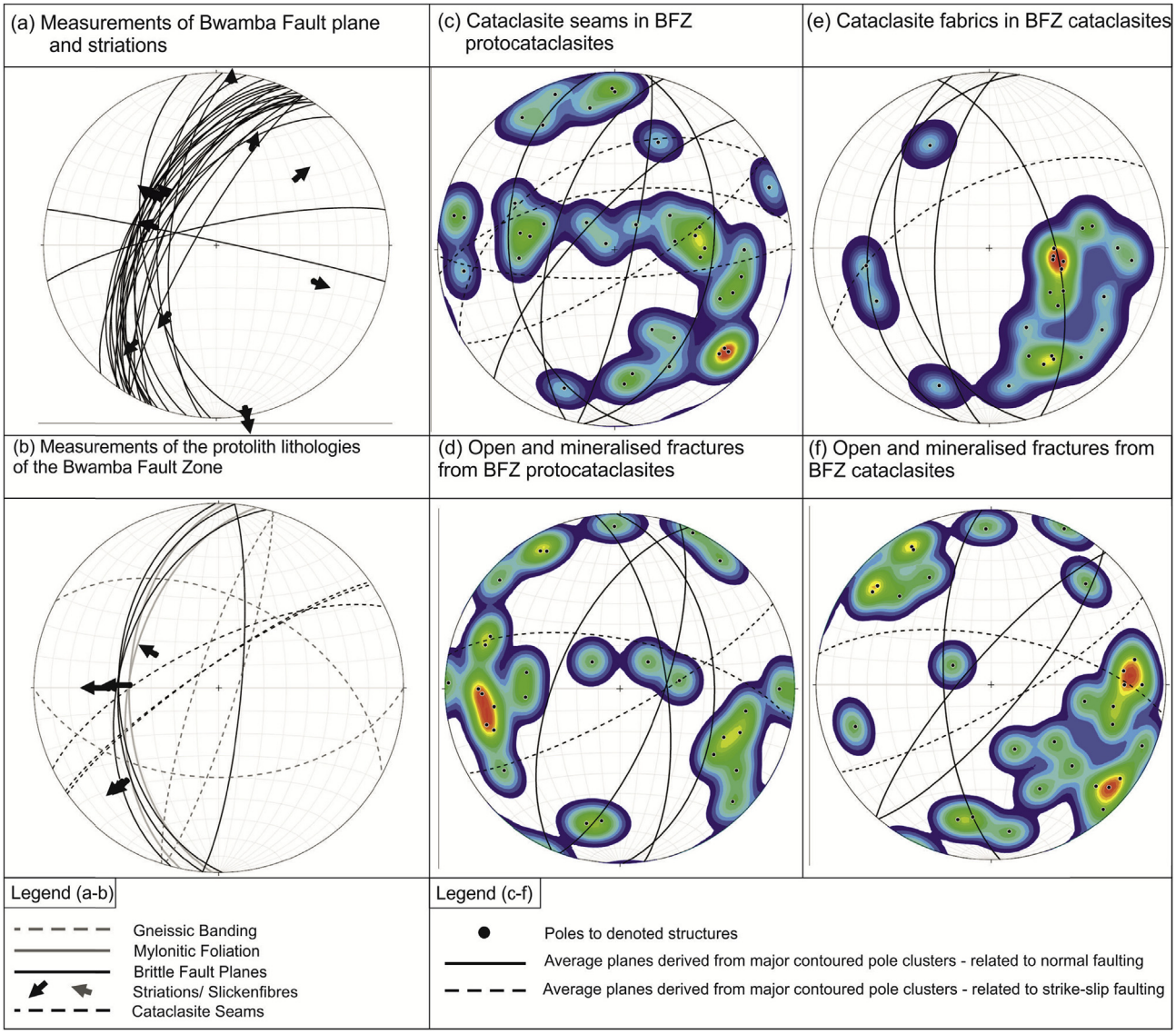

Fig. 2. a) Measurements of slip surfaces and slip vectors in the BFZ at Sempaya. Major NNE-SSW slip surfaces set hosts pure extension, oblique, and pure strike-slip behaviour. Minor E-W striking faults show oblique slip behaviour; b) Structural fabrics within the Aruan Gneiss protolith of the BFZ, showing pre-rift ductile fabrics, and Bwamba Fault-related brittle structures and slip vectors; c) orientations of cataclasite seams within the protocataclasite units (2–6) of the BFZ; d) orientations of fractures and veins with no evidence of shear in protocataclasites; e) cataclasite shear fabrics in cataclasites of the central fault core (unit 7); f) fractures and veins with no evidence of shear in unit 7 cataclasites.

has no basement or fault rock exposure.

The Bwamba Fault scarp has an average orientation of 203/55° WNW (Fig. 2a) and exhibits largely dip-slip extension, with rare oblique dextral and sinistral strike-slip indicators (Fig. 2a). The latter are related to minor faults constrained within fault-rock lenses tectonically juxtaposed with the main fault scarp by a normal fault at locality C.

The fault zone is composed of several juxtaposed units of fault rocks with distinct lithological and structural characteristics, and fluid-rock interaction textures (Table 1; Fig. 3). Some are correlated along strike and some appear discontinuous. The main fault scarp is the upper surface of the fault core (unit 7); exposures of units 1–6 are exposed east of the fault scarp where erosion of the scarp has occurred, whilst units 8 and 9 are fault-rock lenses attached to the fault scarp.

The damaged protolith in the footwall of the BFZ is composed of granitic to intermediate gneiss (Table 1), It is exposed at locality B within the fault zone, and locality D within the damage zone. Gneissic banding is oriented WNW/ESE and characterised by tight, south-verging folds (Fig. 2a). These orientations are at high angle to the Bwamba Fault, indicated by orientations of fault-parallel cataclasite-bearing microfaults that cross-cut the gneisses (Fig. 2b). Fractures and Fe-oxide veins also cross-cut the gneiss, which are oriented sub-parallel to both gneissic-banding, and the Bwamba Fault (Fig. 2a). At locality E basement fabrics are parallel to the Bwamba Fault orientation, and are defined by strongly foliated amphibolites that have undergone partial retrogression that produced aligned muscovite and chlorite. The amphibolites are tightly folded, with limbs oriented 198/80° and 017/82°, and the gneissic banding surfaces are characterised by dextral slickenlines and quartz slickenfibres plunging ~30°→ 225 (Fig. 2c). Overlying the metabasites are mylonitic quartzo-feldspathic gneisses with aligned retrograde phyllosilicates mantling foliation planes. The mylonitic foliation is also oriented parallel to the Bwamba Fault (~190/50°), and hosts dip-slip, normal slickenlines that plunge ~ 50° → 270 (Fig. 2c). Only the samples of host-gneiss within the fault zone at locality B (Sempaya) are described below.

Protocataclasites in units 2–6 have experienced rift-related fracturing, comminution and fluid-rock interaction during the evolution of

Table 1
Lithological descriptions of discrete units within the Bwamba Fault Zone as depicted visually in Fig. 3. Units are referred to by this code in the text.

Fault zone unit	Lithological description
1	**Granitic Gneiss** cut by Fe-oxide-mineralised and non-mineralised ultracataclasite
2	**Metabasic Protocataclasite** blocks, cut by K-feldspar, carbonate and Fe-oxide-rich carbonate veins
3	**Porous Protocataclasite** composed of albite gneiss, cut by haematite and jarosite-bearing ultracataclasite seams, K-feldspar, quartz and Fe-oxide veins
4	**Heavily Fe-oxide-mineralised Protocataclasite** composed of sericitised and carbonate-replaced feldspar clasts, and Fe-oxide-rich ultracataclasite with a strong cataclastic fabric
5	**Felsic Protocataclasite**, with intermittent jarosite-bearing cataclasite ultracataclasite layers
6	**Foliated Protocataclasite** composed of felsic gneiss and replacive carbonate, punctuated with cm-wide cataclasite seams with strong cataclastic fabric
7	**Cataclasite** and Ultracataclasite composed of gneiss, mylonite and reworked protocataclasite clasts, enveloped by a quartz + feldspar matrix. Has a strong fabric defined by banding and Fe-oxide precipitation in cataclastic fabrics
8	**Protocataclasite Fault-Rock Lens**; Fe-oxide mineralisation of protocataclasite matrix composed of carbonate-replaced feldspar and quartz, crosscut by later minor faults
9	**Cataclasite Fault-Rock Lens** composed of rounded gneiss and mylonite clasts in a quartz and feldspar matrix. Fe-oxide mineralisation occurs cataclastic fabrics

the Bwamba Fault. Each unit is between 1 and 2 m thick, and separated by fault-parallel Fe-oxide veins. Units 2 and 3 are exposed at locality B, in close proximity to the exposure of granitic gneiss (unit 1); the upper boundary of unit 3 is gradational with the laterally continuous fault core (unit 7). Units 4, 5 and 6 occur adjacent to one another at locality A, and are bounded by fault parallel Fe-oxide veins; these surfaces lack evidence of slip direction. The boundary between unit 6 and the fault core (unit 7) is not exposed.

Protocataclasite (units 2–6) are characterised by a series of variably oriented cataclasite and ultracataclasite seams. Fault parallel seams are oriented ca. 196/61° – 225/71°, depending on the variable orientation of the Bwamba Fault along strike (Fig. 2d). A moderate west-dipping cataclasite fabric (ca. 175/41°), and a moderate (ca. 011/44°) and steep (012/83°) east-dipping fabric (Fig. 2d) are also present. Additionally, there is a fault-perpendicular E-W steeply-dipping cataclasite fabric (Fig. 2d). Similar structural geometries are observed in Fe-oxide and quartz veins and fractures that show no evidence of comminution or displacement (Fig. 2e). A fault parallel vein and fracture set (ca. 206/58°) is present, along with a conjugate east-dipping set of veins and fractures (ca. 359/71°) (Fig. 2e). There is also an ENE-WSW set of veins

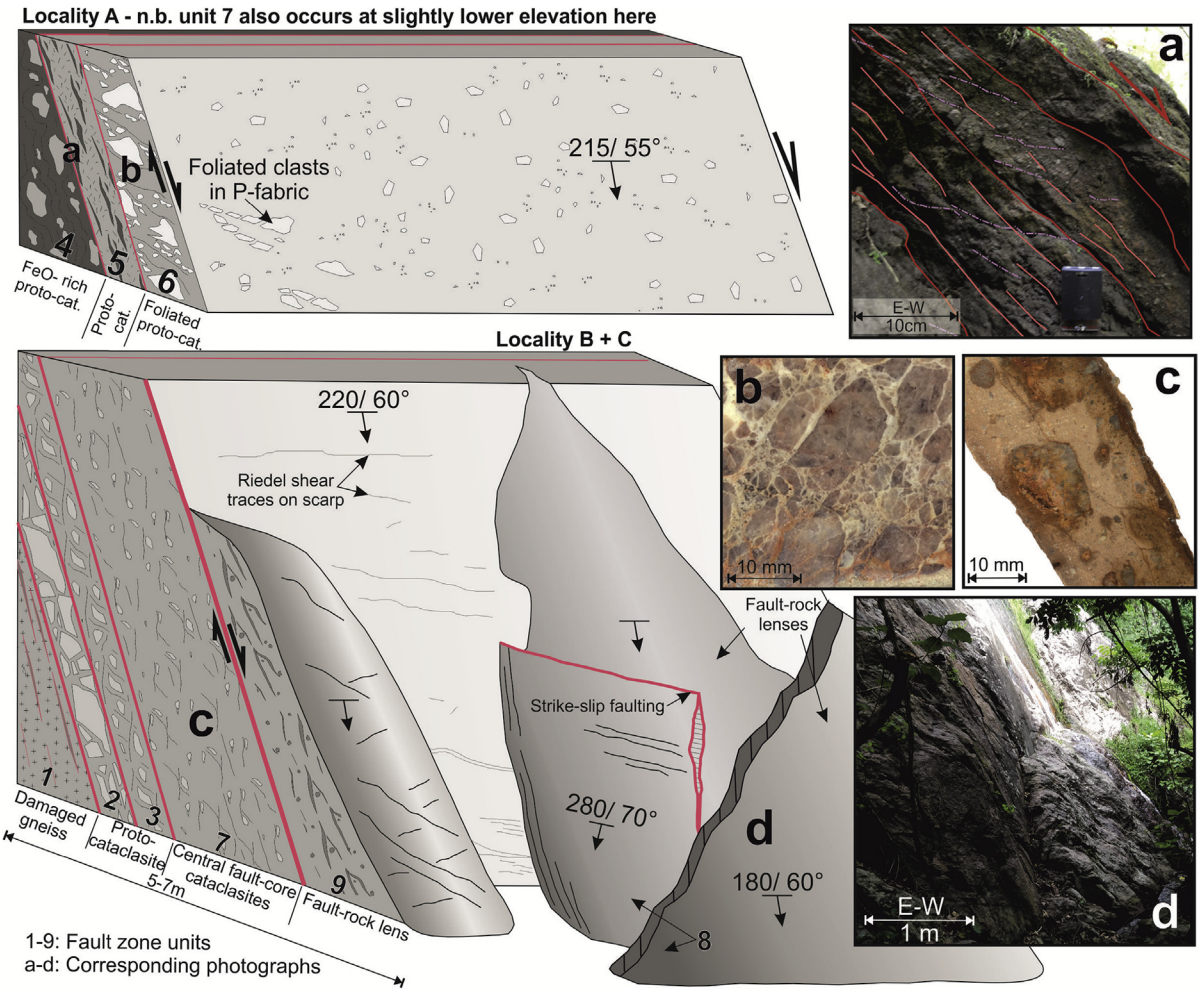

Fig. 3. Graphic representation of the studied exposures of the Bwamba Fault Zone, showing the spatial relationships and general textural characteristics of discrete fault zone units, photographs accompanying sketch are a) Coherent brittle fabrics within fault zone units 4–6; b) representative textural characteristics of proto-cataclasite BFZ units; c) representative textural characteristics of cataclasite BFZ units; d) Geometry of fault-rock lenses overlying the scarp of the Bwamba Fault.

and fractures that have similar geometries to the E-W cataclasite seams (Fig. 2e).

The fault core (unit 7) is composed of cataclasites with 10–30% survivor clasts derived from the gneissic protolith, ranging between sub-mm and 10s of cm. It is between 1 and 3 m thick and is laterally continuous across localities A-C over ~600 m. The scarp hosts dip-slip striations plunging ~60° → 290. The strike of the fault scarp shows variations between NE-SW and N-S across a few 10s of metres. Similar Fe-oxide veins and cataclasite seams to those found in the protocataclasites are present. Cataclasite seams are largely parallel to the scarp between ~171/50° - ~243/60° (Fig. 2f). A W/WNW-dipping cataclasite fabric is also present (Fig. 2f). Veins and fractures cross-cutting the cataclasites generally strike either subparallel to the fault, steeply NW or SE dipping (likely tensile fractures), or WSW-ENE trending (Fig. 2f).

Overlying the fault scarp are two rhombohedral "lenses" (units 8 and 9) of tapered, coherent blocks of fault rock. These are in faulted contact with the major scarp based on dip slip striations at the contact. Each lens has a distinctive lithology and has a maximum thickness of 1–2 m. Unit 8 is cut by a normal fault (202/65°) and a strike-slip fault (280/70°) that abuts against the normal fault (Fig. 3). The geometry of the strike-slip faulting observed is consistent with the prominent WSW-ENE trending fractures, veins and cataclasites fabric throughout the BFZ (Fig. 2). The hanging wall fault-rock at locality C is the westernmost exposed unit of the fault zone. The travertine deposits of the Sempaya Hot Springs are located at N 0°50′06.49″ E 30°09′55.44″.

3.2. Petrographic and microstructural analyses of Bwamba Fault Zone units

3.2.1. Micro-faulted granitic gneiss

The granitic gneisses forming the protolith of the BFZ are composed of quartz (40%), altered plagioclase (40%) and orthoclase feldspar (10%), biotite (5%), Fe-oxides, and trace amounts of zircon. Gneissic banding (cm-scale) is defined by alternating coarse-grained (2 mm) and finer-grained (~0.5 mm) layers. Quartz contains planes of ~0.3 mm fluid inclusions, Fe-oxide- micro-quartz– and muscovite-bearing veins, partially-healed fractures, open tensile fractures (Fig. 4a), and significant subgrain development. Grain boundaries show Fe-oxide precipitation.

Original plagioclase is albitised and sericitised (Fig. 4). Sericite and Fe-oxide precipitation along twin planes is common. Fe-oxide veins are absent in albite, and quartz-hosted Fe-oxide veins terminate at quartz-albite boundaries, resulting in fan-shaped precipitations of Fe-oxide (Fig. 4b). Several ~0.2 mm concentric pores occur within plagioclase, more commonly in the finer-grained bands. Micro-pore margins are frequently mineralised by Fe-oxides. Similar alteration and mineralisation textures occur within orthoclase. Biotite has largely been replaced by Fe-oxide, identified only by relict cleavage planes.

Fe-oxide is most abundant within micro-fault zones, occurring along the edges of ~0.25 mm elongate pores, and as pore-filling cement in ultracataclasite (Fig. 4c). Micro-fault zones are ~5 mm across, and grade from protocataclasite into 1 mm ultracataclasite cores, composed of ~10 μm quartz and feldspar (Fig. 4c). Fault cores anastomose and enclose grains of the protolith between strands (Fig. 4c) and are connected via the network of cross-cutting Fe-oxide veins (Fig. 4a).

3.2.2. Protocataclasite

Protocataclasites observed proximal to the microfaulted gneisses at locality B include 10–20 cm blocks of metabasic protocataclasite (unit 2), and porous felsic protocataclasite (unit 3) that are juxtaposed between seams of very fine-grained cataclasite matrix (Table 1; Fig. 3). Metabasic blocks are composed of 1 mm albite with ~5% 20–50 μm muscovite inclusions, and partially chloritized hornblende (Fig. 5a). Chloritization occurred along hornblende cleavages (Fig. 5a&b). K-feldspar occurs at the margins of such veins, with calcite, dolomite, and Fe- and Mg-rich carbonates typically present in the central portions (Fig. 5a&b). Veins are typically 100–750 μm wide. Felsic gneiss blocks in the cataclasite are composed of albite and lack hornblende and biotite. Albite (~1 mm), contains ~100 μm micropores (Fig. 5c), and 20–50 μm K-feldspar inclusions (Fig. 5c). K-feldspar mantles albite grain boundaries and also occurs in ~ < 10–20 μm veins that crosscut the matrix. The matrix is also cut by veins and ~1 mm ultracataclasite seams (Fig. 5c&d). The latter may be mineralised by Fe-oxides, or highly porous and non-mineralised (Fig. 5e). Ultracataclasites are composed of ~5–20 μm quartz, albite and K-feldspar. Porous cataclasites contain ~5–10% 5–10 μm jarosite (Fig. 5d), whilst mineralised ultracataclasites contain no jarosite.

Felsic gneisses contain various veins that form parallel to (Figs. 2eand 5c), or conjugate (Fig. 2d) to the fault plane. Veins are often located on the boundary between altered protolith and ultracataclasite seams, some of which originally formed along these structural fabrics (Figs. 2d and 5c&f). In addition to K-feldspar veins, quartz and Fe-oxide veins are present (Fig. 5c–e); Carbonates are not present in felsic gneiss blocks or cataclasites. Fe-oxide veins may cross-cut the quartz veins at small angles, but are generally sub-parallel and follow the edges of the quartz veins. The boundaries between the ultracataclasite and protolith are also frequently characterised by elongate pores that are typically coated in Fe-oxide. The Fe-oxides include haematite, although other Fe-oxides may be present. Framboidal haematite shows geopetal textures in the pores of some wider ultracataclasite seams bound by Fe-oxide veins (Fig. 5e). The thickness of the pore-coatings decreases in an up-dip direction, until only the down-dip side of pore walls is coated at the mineralisation front (Fig. 5e).

Protocataclasites (units 4, 5, and 6 at locality A) are also characterised by Fe-oxide and jarosite mineralisation in cataclasite seams and fractures. These units feature a well-established brittle fabric defined by cataclasite development around blocky or rounded survivor clasts, some of which host Fe-oxide and jarosite mineralisation (Fig. 5f–h).

Protocataclasite is the easternmost unit at locality A (unit 4: Table 1; Fig. 3) and composed of 2–5 cm, orange, well-rounded clasts of extensively sericitised, Fe-oxide mineralised gneiss, separated by strands of black ultracataclasite and Fe-oxide veins. Fe-oxide has completely filled micropores in the altered gneiss and cataclasite, growing in 0.5–1 mm framboidal haematite clusters. The boundary with the felsic protocataclasite (unit 5, Fig. 3) is defined by an Fe-oxide mineralised slip surface.

The felsic protocataclasite (unit 5) is composed of mm-cm angular 1–3 mm grains of quartz, sericitised albite and biotite (Fig. 5f&g). The size and abundance of fragments decreases with proximity to ultracataclasite seams. Albite contains 10–30 μm intra-grain pores. Some grains contain ~20 μm plates of muscovite or euhedral laths of K-feldspar. Quartz exhibits undulose extinction and sub-grain development, and has a similar microporous texture to albite. Biotite forms clusters of 1 mm plates, aligned parallel to cataclasite boundaries, and along grain boundaries of albite and quartz (Fig. 5f). This protocataclasite contains significant jarosite with minimal Fe-oxides (Fig. 5g). Survivor clast grain-boundary pores host spider-web textured jarosite, whilst 5–10 μm microfractures in mosaic-brecciated clasts are mineralised with jarosite. In the discontinuous cataclasite seams that surround survivor clasts, jarosite forms a similar texture to that found in the porous protocataclasite (unit 3), forming 5–10 μm round grains (Fig. 5g). In unit 5 however, there is a higher proportion of relict clasts in the cataclasite matrix, and there is a distinct mm-scale layering defined by jarosite-rich and jarosite-poor layers. Jarosite-rich layers are typically located along the margins of cataclasite seams, adjacent to protocataclasite domains (Fig. 5g). The proportion of matrix to clast increases towards the fault core into a well foliated cataclasite (unit 6: Table 1, Fig. 3), as does the width of cataclasite and ultracataclasite strands relative to protocataclasite domains.

The foliated protocataclasite (unit 6) (Fig. 3) is composed of 2–10 cm angular, blocky clasts of fractured granitic gneiss. The clasts

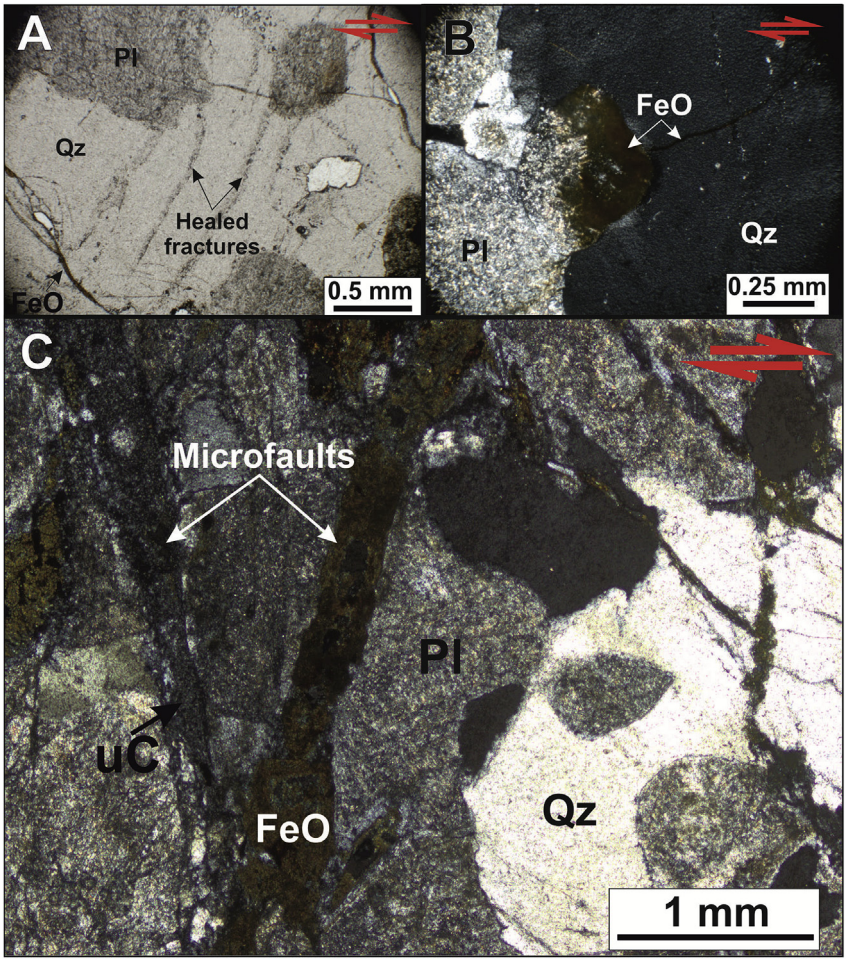

Fig. 4. Photomicrographs in crossed polarized light of deformation textures in granitic gneiss protolith from unit 1 (uC = ultracataclasite, Pl = plagioclase, Qz = quartz, FeO = Iron) n.b. displacement indicators show kinematics of Bwamba Fault; A) Healed fractures and transgranular Fe-oxide veins in quartz with sericitised plagioclase; (B) Abutment of Fe-oxide vein at quartz-plagioclase grain boundary, resulting in fan-shaped mineralisation geometries in plagioclase; C) Bwamba Fault-perpendicular, ultracataclasite-bearing conjugate microfaults, one of which has experienced Fe-oxide mineralisation.

typically have jigsaw-fit geometries separated by 1–5 mm cataclasite strands with ~70% < 1 cm clasts (Fig. 5h). These protocataclasite blocks have well-defined, straight edges with 5–10 cm cataclasite and ultracataclasite strands (Fig. 5h). The clasts are composed of 1–3 mm quartz with undulose extinction, and partially sericitised plagioclase. Plagioclase has also been partially replaced by ~20 μm calcite and dolomite adjacent to 0.5–1 mm carbonate veins (Fig. 5h). These veins are often lined with Fe-oxide, and contain < 100 μm fragments of plagioclase and quartz. The cataclasite and ultracataclasite matrix is composed of 5–40% sub-angular - rounded < 250 μm fragments of plagioclase, quartz, biotite and muscovite, and 60–95% < 20 μm matrix, composed of similar material, but with additional calcite and dolomite. Close to protocataclasite domains, and particularly along the straight edges of cm-sized survivor clasts, significant Fe-oxide vein mineralisation is present. Such Fe-oxide typically has a diffuse front with the ultracataclasite matrix. The clast-to-matrix ratio decreases substantially towards the protocataclasite boundaries (Fig. 5h). Protocataclasite domains are less abundant westward towards the fault scarp, and there is a transition toward cataclasites that form the fault core (unit 7) (Table 1; Fig. 3).

3.2.3. Cataclasite and ultracataclasite

The laterally continuous cataclasites of the fault core (unit 7) are composed of three main components: gneiss survivor clasts, reworked cataclasite fragments, and a cataclasite and ultracataclasite matrix (Fig. 6 a&b). Gneiss clasts occur as large 1- > 10 cm clusters with rectangular-oblate morphologies (Fig. 6 a&b), composed of quartz and albitised and sericitised feldspar, as well as mylonitic clasts composed of recrystallised quartz (Fig. 6b&c). The mm-size clasts in the matrix show a greater degree of rounding than those in the protocataclasites (Fig. 6b). Riedel and P- fabrics that hosted comminution and Fe-oxide precipitation within the existing cataclasites are present and indicate local reworking (Fig. 6a). The easternmost exposure of this unit is a reworked cataclasite with a strong R-P fabric composed of 3–15 mm wide strands of Fe-oxide-rich cataclasite containing < 1 mm sub-angular - rounded quartz and feldspar clasts in a fine-grained (< 20 μm) matrix (Fig. 6a). The development of this fabric generated rhomb-shaped survivor clasts that show top-to-the-west displacement on P-surfaces that displace previously established Riedels (Fig. 6a). Fe-oxide is restricted to the P and R fabrics, and does not occur in the previously formed cataclasite and protocataclasite clasts that were cut by later deformation (Fig. 6a).

The westernmost exposure of the fault core contains 60–95% matrix composed of < 20 μm quartz and feldspar, and 5–40% rounded, fractured cm–dm scale survivor clasts derived from gneiss and quartz mylonites (Fig. 6b). The abundance of survivor clasts decreases to the west, and structural fabrics also become less pronounced. The edges of survivor clasts and strain shadows frequently host Fe-oxide, as do fractures cross-cutting the matrix (Fig. 6b). Fe-oxide veins typically have a "bleed" texture with the matrix, forming a diffuse front 0.2–0.3 mm away from the edges of survivor clast margins and the veins (Fig. 6b).

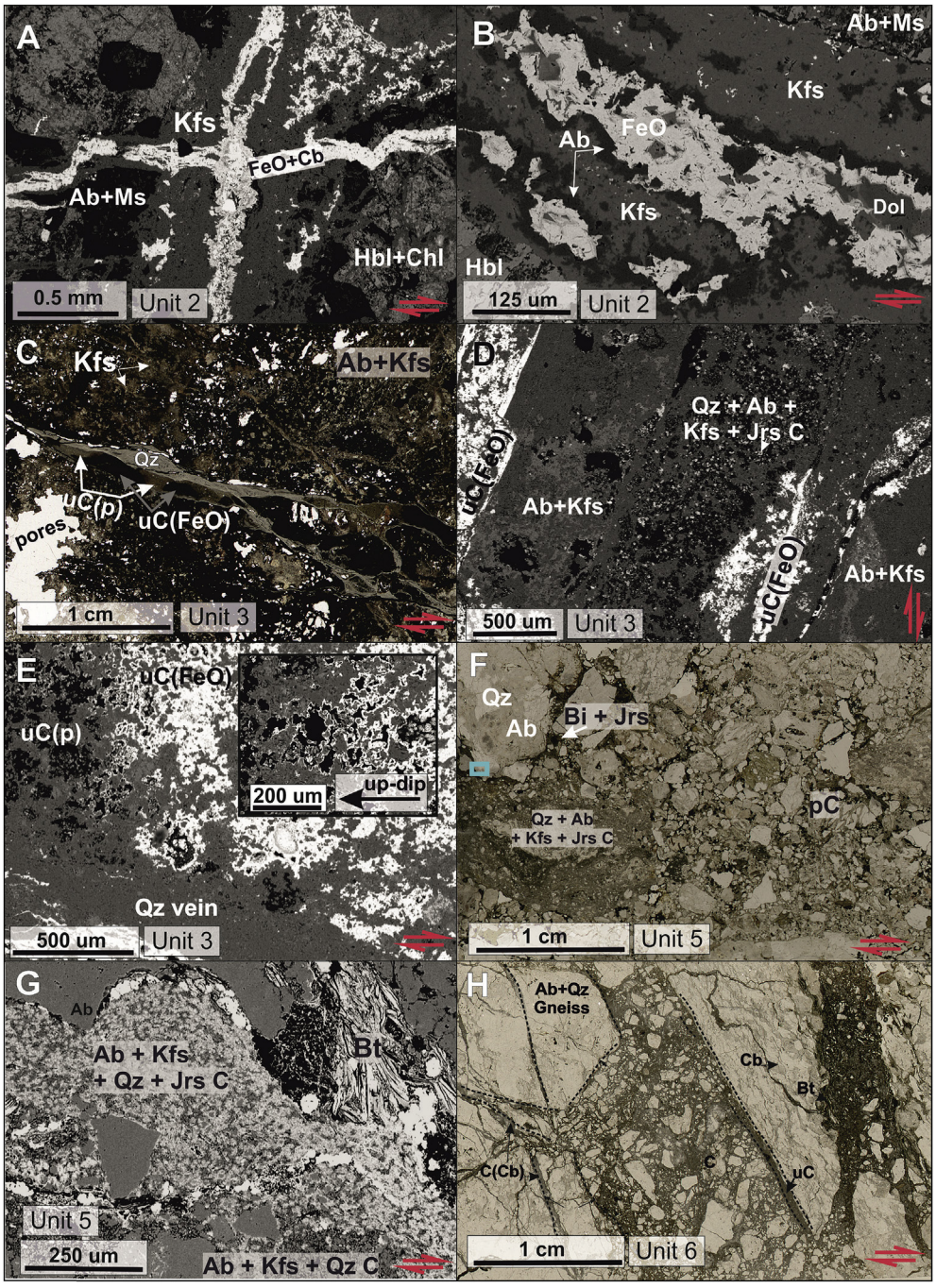

Fig. 5. Backscattered electron (BSE) and secondary electron microscope (SEM), and scanned thin section photographs from protocataclasites in the BFZ (uC(p) = porous ultracataclasite, uC(FeO) = Fe-oxide mineralised cataclasite), Ab = albite, Ms = muscovite, Cb = calcite, FeO = Iron Oxide, Kfs = K-feldspar, Dol = dolomite, Qz = quartz, Jrs = jarosite, C = cataclasite, Bt = biotite): A) BSE image of multi-generational fluid-rock interaction in unit 2. Early greenschist-facies retrogression textures were followed by the development of K-feldspar and Fe-Oxide/carbonate veins during brittle rift-related faulting; B) BSE image showing detail of veining in unit 2. Multiple generations of mineralisation resulted in the formation of K-feldspar, albite, dolomitic carbonate and Fe-oxide veins; C) Photomicrograph of thin section from unit 3 showing the units complex fluid-rock interaction history of felsic gneiss-derived protocataclasite. Replacive albite and K-feldspar host-gneiss was crosscut by porous cataclasite seams followed by quartz veining. Fe-oxide veins that cross-cut prior structures veins were accompanied by partial infill of cataclasite pores by Fe-oxide and jarosite; D) BSE image showing fluid-rock interaction textures in unit 3. From left to right: Fe-oxide-mineralised cataclasite; porous albite + K-Feldspar; Jarosite-bearing porous cataclasite; Fe-oxide-mineralised cataclasite; fractured, Fe-oxide mineralised albite + K-Feldspar gneiss; E) BSE image showing geopetal textures that indicate up-dip fluid migration, resulting in Fe-oxide mineralisation in unit 3, inset photomicrograph shows higher resolution mineralisation front; F) Photomicrograph of jarosite-bearing protocataclasite in unit 5 showing development of microfault zones hosting ultracataclasite; G) BSE image of area highlighted in (F) of unit 5, showing intense jarosite precipitation at margin of developing ultracataclasite seam, dissipating away towards the centre of the microfault core; F) Photomicrograph showing cataclasis and grain fragmentation in unit 6, Fe-oxide rich domains occur along survivor clast edges, as do areas of most intense comminution. Black dashed lines indicated where shearing and wear has occurred along clast margins or microfaults.

3.2.4. Fault-rock lenses

The two fault-rock lenses (unit 8 & 9; Table 1; Fig. 3) are in faulted contact with the main fault scarp. Unit 8 (Table 1) is an Fe-oxide-mineralised protocataclasite, composed of angular ~3 mm fragments of albite and quartz (Fig. 6d). Albite has been partially replaced by calcite, which occurs in clusters of < 0.2 mm grains along twin planes. Fe-oxide is common in the matrix in comparison to the fractured 2–3 cm gneiss survivor clasts, and this unit has experienced more complete mineralisation than other fault-zone components (Fig. 6d). The Fe-oxide-rich protocataclasite is cut by hairline fractures with various orientations, including fractures at shallow-angles (15-30°) to the main fault, and some orthogonal to it that occasionally show more intense Fe-oxide precipitation and further comminution (Fig. 6d). A 0.2–0.5 mm cataclasite and ultracataclasite seam oriented parallel to the fault surface is observed to cut the protocataclasite (Fig. 6d). The ultracataclasite that forms within this microfault exhibits Riedel shears that dip at shallow angles (~20°) to the fault surface.

The cataclasite lens (unit 9) is composed of 0.1–5 mm sub-angular to well-rounded gneiss and quartz-mylonite survivor clasts (Fig. 6c). These clasts constitute ~10% of the rock and are supported by < 50 μm matrix. This unit hosts 0.2–10 mm discrete cataclasite bands defined by variations in matrix grain size and clast proportions (Fig. 6c). Greenish bands contain < 5% clasts and finer grained matrix, whilst beige bands are composed of 30–40% clasts. This banding is oriented between 15 and 30° to the fault orientation, and often the boundaries between bands are associated with Fe-oxide veins (Fig. 6c). Fe-oxide veins are < 0.1 mm thick, and have 0.2–0.3 mm "bleed" textures into the matrix, similar to the textures in the fault core cataclasites.

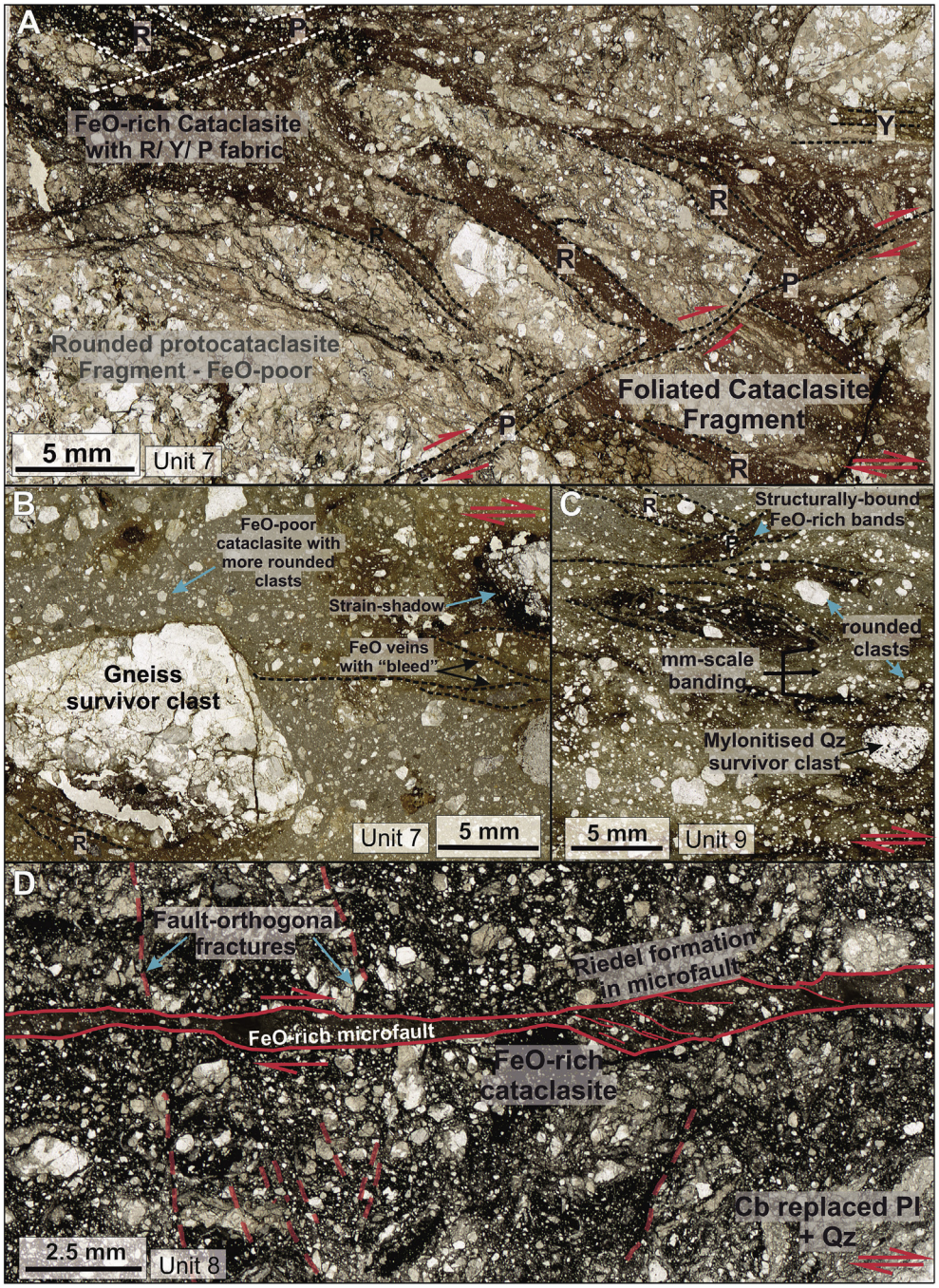

Fig. 6. Scanned thin section photographs of cataclasite units in the BFZ: A) Tectonically reworked protocataclasites in unit 7. Early cataclasis occurred forming foliated and non-foliated cataclasites, these behaved as rigid blocks during a later brittle event, where Riedel and foliation planes (P-planes) were formed in the younger FeO-rich cataclasites. Dashed lines highlight sections of Riedel/P-plane deformation; B) Structurally-controlled Fe-oxide mineralisation in veins and along survivor-clast edges in unit 7. Dashed lines highlight Fe-Oxide mineralisation sites related to structures; C) Structurally-controlled Fe-oxide mineralisation in unit 9 in discrete cataclasite bands at shallow angles to the Bwamba Fault scarp. Dashed lines highlight discrete zones of Fe-Oxide mineralisation; D) Intensely Fe-oxide mineralised cataclasite from unit 8. In addition to the formation and Fe-oxide mineralisation of the cataclasite matrix, further deformation has occurred in the form of conjugate, Bwamba Fault-orthogonal fracturing and microfaulting (dashed red lines). These previous structures were subsequently reactivated by a Riedel-foliated BFZ-parallel extensional fault (solid red lines).

4. Structural evolution, deformation styles and fluid-rock interaction in the Bwamba Fault Zone

The exposures of the BFZ suggest that it is a single core composed of various fault-rock lithologies generated from the comminution of a lithologically homogeneous host rock, similar to the model of Caine et al. (1996). However, discrete "fault strands" with heavily fractured protolith blocks, gouge zones and mineralisation have been observed in similar active rift fault zones that host several km of displacement, and juxtapose crystalline basement rocks with syn-rift-clastic sedimentary units (Kristensen et al., 2016). Although it is possible that the main BFZ hosts subsidiary fault strands in unexposed ground, the BMZ scarp forms the major topographic feature of the basin flank and so is interpreted as the main basin boundary fault. The BFZ, namely the damaged host gneisses, and several discrete fault-core units, presents a rare opportunity to investigate relationship between the structural evolution of a major border fault in the EARS, and the fluid-rock interaction processes.

4.1. Pre-rift metamorphism and retrogression, and syn-rift brittle deformation in the gneiss protolith

The gneisses that form the protolith for the BFZ record high grade amphibolie-facies metamorphic conditions, based on mineral assemblages of hornblende and plagioclase in metabasites, and ubiquitous sub-grain development in quartz. The gneisses also show evidence of pre-rift fluid-assisted retrogression at sub-greenschist to from syntectonic growth of lineated muscovite and chlorite in foliation planes of north-south trending mylonites, and widespread albitization, sericitization and K-feldspar replacement of plagioclase, and chloritisation

of hornblende (Fig. 4). Similar retrograde phases have been assigned to conditions of ~200 °C (Harper et al., 1995). These retrograde phases have been cut by rift-related fractures and faults and are adjudged to have occurred prior of rifting, based also on the brittle reactivation mylonite foliation planes.

Ultracataclasite-bearing microfaults formed parallel to the Bwamba Fault and reactivated the gneissose banding (Fig. 2b). These post-date retrograde metamorphism at even shallower crustal levels. Such faults are correlated with the onset of rifting due to textural similarities with fault-core cataclasites and became pathways for Fe-oxide-bearing fluids in a low permeability protolith (Fig. 4). The Fe-oxide veins that cross-cut the gneiss indicate that fractures provided a permeability network between microfaults (Fig. 4c), where competent quartz hosted discrete fracture propagation, and abutment of fractures at quartz-feldspar grain boundaries occurred. Intensely sericitised feldspars were weaker and did not allow sufficient stress concentration for fracture propagation. The presence of delta-shaped Fe-oxide precipitates at these grain boundary interfaces indicates fluid flow was focussed on fractures through quartz, and diffuse through microporous feldspar.

4.2. Structural fabrics, permeability pathways, fluid-rock interaction and deformation styles operating in the core of the BFZ

4.2.1. Structural fabrics in the fault core

Brittle fabrics in the BFZ have been categorised by both the fault-rock lithology and the evidence of shear (e.g. grain size reduction) (Fig. 2). There is a dominant set of structural fabrics related to extensional faulting (Fig. 7), and a set related to minor strike-slip fault development within the BFZ, consistent across all fault zone units. Establishing consistent cross-cutting relationships is difficult, and we cannot establish the temporal relationship between fabrics of normal and strike-slip origin, however, striations on the fault scarp (Fig. 2a) predominantly indicate dip-slip extension with minor oblique and strike-slip occurrences (Fig. 2a), supported by fault plane solutions derived from seismic event data (Lindenfeld et al., 2012). It is therefore likely that the minor strike-slip fabrics are overprinting a dominant normal fault signature.

Cataclasite seams within all fault core lithologies, in part show fault-parallel fabrics striking between ~170° and ~240° (Fig. 2), with variations ascribed to changing orientation of the Bwamba fault. Fabrics within the fault rocks of brittle shear zones are well established in shallow crustal fault zones (Chester and Logan, 1986; Petit, 1987). In the BFZ, several cataclasite seams, particularly in protocataclasite units (Fig. 2d) are interpreted as; P-foliations which strike between ~175° – 220° and dip ~30° - 40°; Riedel shears which strike ~10° and dip steeply (~80°) east; and R′- foliations strike parallel to Riedel shears, dipping ~ 45° E (Fig. 7). Fault parallel cataclasite seams are considered possible Y-shears. These foliations are slightly oblique to the average orientation of the fault zone (Fig. 7), suggesting that there is a sinistral obliquity to the extensional fabric. This is consistent with stress tensors derived from seismic events in the region (Lindenfeld et al., 2012; Sachau et al., 2016). Some mm-wide cataclasite seams conform with the geometries of minor strike-slip fault geometries (Fig. 2 c-f) and are interpreted to be of strike-slip origin.

Interpreting structures that have no evidence of shear (e.g. veins and open fractures) is more difficult. In addition to fault-parallel, and conjugate (Fig. 2e) veins and fractures, there are ENE-WSW trending conjugate sets, which are likely related to strike-slip faulting, and a further steep NE-SW trending set (Fig. 2g) that are interpreted as tensile structures related to extensional faulting.

4.2.2. Permeability pathways

Mineralisation textures and fluid migration pathways, are intimately associated with structural fabrics in the BFZ. The major fluid pathways in the protocataclasites are inferred from the presence of mineralised fractures, high permeability cataclasite seams, and survivor

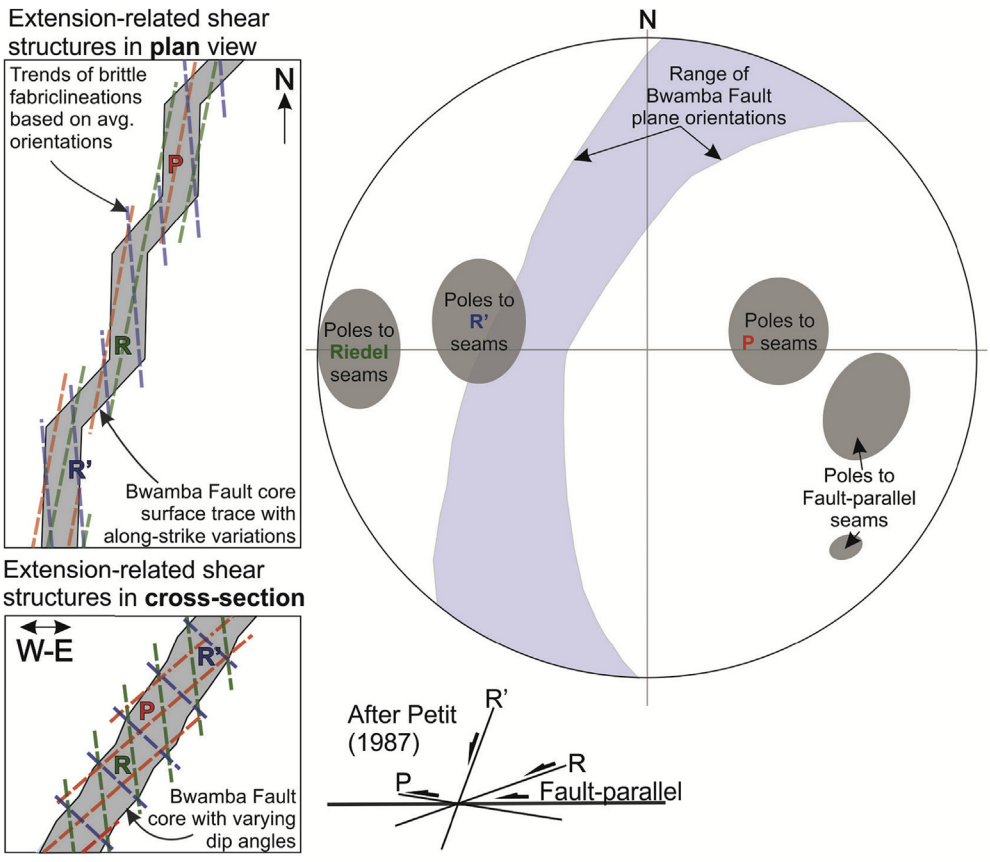

Fig. 7. Interpretation of extension-related shear fabrics within cataclasite seams from the BFZ. Stereonet shows combined average pole clusters from Fig. 2c and e, indicating the presence of Riedel, R′ and P seams within the cataclasite matrix. The left panels graphically depict the expected geometries of these fabrics in map and cross-section view, showing they are slightly oblique to the Bwamba Fault. Strike-slip fabrics are not considered as these kinematics constitute a minor component of the fault zone overall, occurring in localised sections only.

clast edges. The latter possibly formed asperities along brittle structures based on their affiliation with well-comminuted ultracataclasite seams (Fig. 5). The wide-range and intensity of deformation in the protocataclasite units indicates they hosted the most significant fluid flow in the observed components of the BFZ.

Permeability was more restricted in matrix-rich cataclasite (e.g. unit 7) due to a lack of brittle fragmentation and minimal asperity-driven milling. Mineralisation is restricted to Fe-oxide veins that cross-cut the cataclasite (Fig. 6b), or along the edges of rare survivor clasts (Fig. 6b). In this sense, the permeability of well-comminuted fault-rocks became more comparable with the crystalline protolith (c.f. Wibberley and Shimamoto, 2002). As such the best record of fluid-rock interaction in fault zones may be preserved in the damage zone, or chemical alteration zone (Kristensen et al., 2016).

4.2.3. Sequence of rift-related fault-zone mineralisation

Brittle failure and cataclasis in the BFZ facilitated in two distinct fluid-rock interaction events; an early event characterised by localised quartz, feldspar and calcite and dolomite veining, and a later more widespread event characterised by Fe-oxide and jarosite veining and cementation of the cataclasite matrix.

Metabasic protocataclasites host early K-feldspar as both veins and fill of albite micropores (Fig. 5a&b). Such authigenic K-feldspar has been ascribed to temperatures of 100–150 °C (Harper et al., 1995). Carbonate precipitation in the central areas of veins consistently post-dates K-feldspar formation, which may have resulted from an evolving fluid composition where more CO_2 became available, and Ca from plagioclase or hornblende.

Felsic protocataclasites likewise host early K-feldspar veins, followed by quartz veins (Fig. 5d). Quartz veins post-date cataclasite formation as they are localised along cataclasite-protolith clast boundaries (Fig. 5d), and are not reworked. The second event is evidenced by haematite veins and cataclasite pore-filling cements that post-date the formation of cataclasite and quartz veins (Fig. 5d). Geopetal structures indicate that Fe-rich fluids migrated up-dip within the BFZ (Fig. 5e). Fe-rich fluids appear to have interacted variably with the host mineralogies, forming carbonates in metabasic protoliths, and Fe-oxides and hydrothermal jarosite in the more felsic units.

Hydrothermal jarosite in felsic gneiss cataclasites indicates the interaction between Fe-rich fluids and host cataclasites, and is interpreted as a late stage precipitate, forming either simultaneously with, or post-dating, Fe-oxide veining. Hydrothermal jarosite has been observed in other rift-fault zones, associated with steam-heating in the shallow crust and acidic conditions caused by the oxidation of H_2S derived from rift-basin sulphates at temperatures of ~180 °C (Lueth et al., 2005).

The central fault core cataclasites and ultracataclasites lack the complex mineralisation history of protocataclasite units, hosting only Fe-oxide and limited jarosite veining with minor bleed textures. Coupled with evidence from this unit of reworking of fault-zone rocks as survivor clasts, this suggests that it may only have experienced the late influx of Fe-rich fluids, and that permeability was more restricted in the central fault core relative to protocataclasites. Typically the finest grained matrix of fault core rocks yield low permeability values (Wibberley and Shimamoto, 2002), suggesting fluids had more limited access to the central core of the BFZ than protocataclasite units. The fault lenses have experienced early replacement of plagioclase by calcite, followed by more significant Fe-oxide mineralisation of structural fabrics and the cataclasite matrix (Fig. 6 d&d).

4.2.4. Deformation styles

Shearing and cataclastic flow were originally operating simultaneously in the protocataclasite units (units 2–6). Thus shearing occurred along the boundaries of survivor clasts, causing comminution and grain size homogenisation, whilst cataclastic flow occurred between survivor clasts, resulting in a wide particle size distribution. The development of granular cataclasite aggregates between blocks signifies a transition from brittle failure toward cataclastic flow due to gradual removal of asperities and a decrease in clast: matrix ratio (Sibson, 1977). Whilst there is evidence of frictional sliding along, and fragmentation of, survivor clasts that led to increased permeability and Fe-oxide mineralisation in the cataclasites of the fault core (Fig. 6b&c), the dominant deformation mechanism in these rocks was likely rotation, sliding and dilation of the angular ultracataclasite matrix, processes that have been observed in natural and laboratory-generated brittle shear zones (Chester et al., 1985; Mair et al., 2002).

Fragmentation and fracturing of gneiss blocks was a more significant permeability-creating process than flow within the porous cataclasite matrix. Fractures and survivor clast boundaries are frequently coated with Fe-oxide and jarosite, whilst the cataclasite matrix generally lacks Fe-oxide mineralisation, though there are some examples of partially or completely mineralised ultracataclasite seams (Fig. 5), or more widespread matrix mineralisation (units 4 & 8). Permeability reduction of porous granular aggregates subject to cataclastic flow (Zhu and Wong, 1997) suggests that if the yield stress of the ultracataclasites was not reached, their permeability was lower than brittle-behaving survivor clasts. In the case of the BFZ, it is evident that the yield stress of both protocataclasites and cataclasites was exceeded, as they are commonly cross-cut by veins (Fig. 5c; Fig. 6b) indicating a switch from cataclastic flow to brittle failure. The development of cataclasite and gouge in the BFZ with a wide particle size and angular grains, may promote frictional strengthening of the fault zone, and facilitate stress concentration and eventual failure along such discrete surfaces (Mair et al., 2002).

4.3. Structural and hydrogeological evolution of the Bwamba Fault Zone

4.3.1. Geometrical and mechanical development

Pre-rift structural fabrics are thought to influence the initiation and development of rift segments to varying degrees in the EARS (Hodge et al., 2018), and in other rifts (Salomon et al., 2015). The reactivation of gneiss fabrics may have been a factor in the development and evolution of the Bwamba Fault. Whilst gneissose banding is oriented perpendicular to the Bwamba Fault at Sempaya (Fig. 2b), the development of a strong fault-parallel mylonitic fabric prior to the onset of rifting may have locally controlled fault geometry (Fig. 2c). The presence of aligned, retrograde phyllosilicates within this mylonitic zone may have encouraged strain localisation (c.f; Holdsworth et al., 2001; Holdsworth et al., 2011). Proximal to the fault core, phyllosilicate-rich metabasites and mylonite foliation surfaces host both dextral strike-slip and normal slickenlines with quartz slickenfibres that have identical orientations to those in the fault core (Fig. 2 a&c). The extent to which pre-rift structures controlled the geometry of the whole Bwamba Fault is uncertain. It is possible that it may only be a local controlling factor (e.g. Hodge et al., 2018).

Once the BFZ was established, lithological, structural and permeability characteristics were variable between individual units. It is possible that the different fault zone units formed during successive stages of the mechanical and geometrical evolution, and that this has resulted in fault zone compartmentalisation, with each unit hosting variable hydraulic properties. The thickness of the core components (fault rocks) may increase due to areas of overlap, such as relay zones. The generation of new slip-surfaces, or the localisation of deformation on existing slip-surfaces will facilitate further slip (Childs et al., 2009). The juxtaposition of different fault zone units may be the product of successive strain partitioning across new and or existing slip surfaces. This may be governed by the geometry of the footwall slip-surface (Childs et al., 2009), the lithological or tectonic-influenced fault-strengthening processes, such as the silicification and cementation of cataclasites during interseismic periods (Tenthorey and Cox, 2006). This may result in the partitioning of strain across several slip-surfaces, rather than localising strain on a single, through-going, weak slip-surface. Well-foliated phyllosilicate minerals are often ascribed to be a key

factor in strain localisation and fault-weakening behaviour (Lawther et al., 2016). However their absence in the BFZ may promote relatively strong fault rocks (Ikari et al., 2011).

The fault-rock lenses (Units 8 and 9) are suggested to have formed from the successive growth of the BFZ, based on their geometric and tectonically-controlled relationship with the main fault scarp. They also show evidence of more recently generated microfaults cross-cutting existing cataclasites (Fig. 6d), indicating further deformation took place.

4.3.2. Temporal relationship between fluid ingress and fault zone development

Establishing a precise temporal sequence between fluid ingress and the structural development of the BFZ is difficult. However, the sequence of mineralisation of fault rocks (section 4.2.3) allows for some temporal relationships to be established.

We propose two end-member cases for the relationship between fluid influx to the BFZ, and its relationship to the structural development of the fault zone. In the first case, fluid ingress is considered to be synchronous with structural developments such as brittle fracturing, and the development of Fe-oxide mineralisation. Several faults in different tectonic regimes show evidence of stress cycling in which earthquake behaviour is intimately linked with fluid pressure and fault zone permeability (Cox, 1995; Sibson, 2007; Japas et al., 2016). Fault-valve mechanisms host fluid pressure accumulation during the interseismic phase between earthquakes, and expel fluids during co-seismic rupture (Sibson, 1990). The opening of fractures and dilating cataclasite seams during coseismic phases of the BFZ may have permitted the drawing-in and upwards-migration of mineralising fluids. These formed veins and Fe-oxide and jarosite mineralisation of cataclasites during ingress events. Such deformation-controlled fluid flow has been modelled numerically, and in a drained dilating fault core with fracture-related and granular matrix permeability pathways, fluids may be drawn into discrete layers coseismically, and expelled during post-seismic compaction (Goren et al., 2010). The process of porosity reduction and lithification of cataclasites may also increase fault-zone strength, allowing for further stress localisation and brittle failure.

The behaviour of the BFZ is not directly comparable to classic models of fault-valve behaviour, which focus on process at the brittle-ductile transition (Sibson, 1990; Byerlee, 1993; Cox, 1995). However the transient drawing in of fluids by fractures and cataclasite seams during extensional dilation, and their subsequent mineralisation, is consistent with fault-valve behaviour at a shallow crustal level. Fluid-triggered seismic behaviour has been documented in the Rwenzori region, further indicating the plausibility for fault-valve behaviour in the BFZ, particularly considering the full extent of the damage zone is not exposed, which may host a more complete fluid-rock interaction record (Caine et al., 1996; Kristensen et al., 2016).

In an alternative scenario, mineralisation along fracture networks may have post-dated the formation of these structures during upward fluid migration in the post/interseismic phase. Textural evidence in the BFZ indicates that fluid migration largely post-dated cataclasite and earlier quartz vein formation (Fig. 5d&e), indicating that existing structures within the fault-zone were important fluid pathways for potential inter-seismic flow. Numerical modelling has shown that upward fluid migration along an active fault may occur in the post-seismic stress recovery period, driven by fluid overpressure from beneath a suprahydrostatic seal (Sheldon and Ord, 2005). A laterally consistent, horizontal sealing layer is possible in the Semliki basin that may experience periodic rupturing and post-seismic upward fluid flow. Alternatively, the potential for overpressure in sealed compartments within the fault zone (i.e. Byerlee, 1993) could develop overpressure, and the ability for the BFZ to host upward migration of Fe-rich fluids; mineralisation of structural fabrics, slip surfaces and particular fault-zone units evident in surface exposures may be responsible for compartment formation at depth.

4.4. Fluid sources in the BFZ, and its role in the Albertine Rift System

4.4.1. Fluid sources for mineralisation of the BFZ

There are three potential fluid sources responsible for the mineralisation that has occurred in the BFZ. The first source is meteoric fluids, which are capable of infiltrating fault zones to mid-crustal levels (Haines et al., 2016), and downward flow may occur in fault zones that lack overpressure (Sheldon and Ord, 2005); this is probably less likely to occur in the BFZ which may have mineralised sealed compartment based on the occurrence of fault zone units with discrete fluid-rock interaction textures. Downward and lateral fluid infiltration in the BFZ has been suggested, which may act as a conduit feeding the Buranga Hot Springs (Fig. 1) with runoff waters from the Rwenzori massif, despite the 60 km distance (Ochmann et al., 2010). However, the identification of potential mineralised seals within the fault zone may prevent effective connectivity of downward migrating fluids. The chemistry of the Buranga Hot Springs indicates they are largely fed by meteoric waters (Bahati et al., 2005), though the presence of CO_2 and helium, and S- and Sr-isotopic compositions of the hot spring fluids (Ochmann et al., 2010) also require the presence of mantle-derived fluids. These should be considered as a potential source for mineralising fluids in the BFZ. The presence of a low-velocity structure directly beneath the BFZ at around 10 km depth is a potential source for such magmatic fluids (Ochmann et al., 2010).

The alkaline chemistry of the hot-spring fluids, in addition to the presence of nearby laterally extensive (~10 km) travertine deposits (Bahati et al., 2005), contrast with our findings of lithologically-restricted carbonate mineralisation in the fault rocks, and evidence of acidic fluid required for the precipitation of jarosite (Lueth et al., 2005). Based on mineralogical, and textural evidence in cataclasites, we propose a third possible fluid source for BFZ mineralisation, formation fluids from the wall-rock, i.e. the Aruan gneisses, and later, the Semliki Rift Basin (Fig. 8).

The occurrence of jarosite and haematite as mineralising phases in the BFZ requires a source of sulphur and iron that are unlikely to be derived from the largely felsic gneissose wall-rock. The Semliki Basin contains abundant Fe-rich mudstones that are associated with significant gypsum and sulphur deposits in the form of complex vein networks (Kiconco, 2005; Roller et al., 2010). Hence rift basin fluids enriched in Fe and S may have utilised the Bwamba Fault as a conduit (Fig. 8). Similar permeability linkages between basin sedimentary rocks and basin-bounding faults have been suggested to occur in the Rio Grande Rift (Lueth et al., 2005), associated with hydrothermal jarosite precipitates, and with hydrothermal dolomite in the Suez Rift, Egypt (Hollis et al., 2017).

Thus, a significant hydrological change occurred between two discrete fluid ingress events in the BFZ. The first event likely involved the drawing in of limited fluids from the relatively impermeable host gneisses whilst this section of the Bwamba Fault was entirely within the basement (Fig. 8a). The second ingress event occurred when the currently exposed section of the fault came into contact with fluids from the Semliki basin during progressive exhumation of the footwall rocks and fault core (Fig. 8b). At this stage the fault became a conduit for basin fluids. Such communication between basin fluids and basement fault may be an important factor in many rift settings.

4.4.2. The Bwamba Fault and its role in the Albertine Rift System

The structural and fluid-rock interaction history of the BFZ has implications for energy resources in the Albertine Rift System. The Buranga Hot Springs have been suggested to be associated with fluid-flow in the BFZ (Bahati et al., 2005; Ochmann et al., 2010). The migration of travertine deposits over ~10 km (Bahati et al., 2005) indicates the evolution of the BFZ may influence the geothermal systems. Several oil seeps have been observed in the Albert Rift to the north associated with active rift faults (Logan et al., 2009), for which the hydraulic properties of the BFZ may serve as an important analogue.

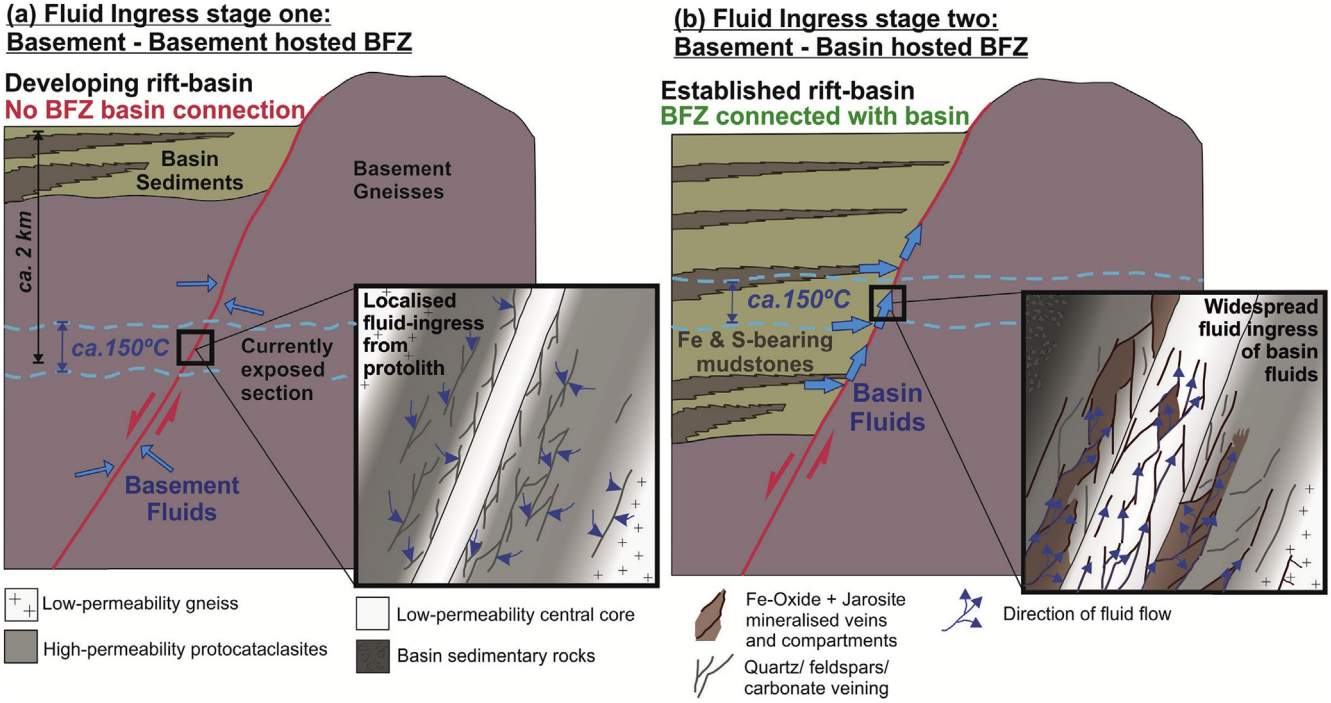

Fig. 8. Hydrological evolution of the BFZ; a) a basement-hosted BFZ experiences vein mineralisation with fluids derived from local sources, i.e. pore-fluids in wall-rock. Protocataclasites record this stage, which is not observed in the central fault core; b) with the establishment of the Semliki Rift, the fault zone comes into contact with Fe and S-bearing basin sediments. A major hydrological shift accompanies this stage, during which widespread fluid ingress occurs in the BFZ of basin fluids that form mineralised compartments and veins.

The Bwamba Fault accommodates the uplift of the western flank of the Rwenzori Mountains, the mechanisms, timings and magnitudes of which are uncertain (Ring, 2008; Koehn et al., 2010; Wallner and Schmeling, 2010; Bauer et al., 2013). The fault has facilitated at least 5 km of displacement, based on the elevation of the Rwenzori Mountains above the Semliki Valley floor (Bauer et al., 2012). Based on an estimated depth to basement in the Semliki rift of between 3 and 6 km (Kiconco, 2005), coupled with uplift above the general rift shoulder, a 10 km maximum displacement has been suggested (Ring, 2008). At Sempaya displacement values are probably lower due to proximity to the fault tip. This is likely to be a minimum estimate, as only a single fault core is exposed, and the extent a damage zone could not be established.

Although estimated conditions of mineralisation from our study, and those associated with cataclasite formation (Sibson, 1977, 2000) provide some temperature constraints, converting these into likely depths of formation is complicated due to uncertainty in the values of geothermal gradients in this rift zone. Estimates of the geothermal gradient for the Albertine Rift System vary from 28 °C/km to 67 °C/km (Abeinomugisha, 2010), with the maximum associated with Buranga Hot Springs. Temperature estimates for the crystallisation of hydrothermal K-feldspar (100–150 °C; Harper et al., 1995) and jarosite (150–200 °C; Lueth et al., 2005), coupled to this range of thermal gradients imply depths of mineralisation from ca. 2–7 km. Cataclasite-series rocks typically form between ca. 4–7 km depths at 30 °C/km (Sibson, 1977, 2000), though locally elevated geothermal gradients would facilitate cataclasis at shallower depths. Therefore, if the surface-exposed cataclasites of the BFZ formed concurrent with coseismic fluid injection, or shortly prior to up-fault post-seismic fluid migration over 10s of years (Sheldon and Ord, 2005), then minimum displacement values of ca. 2 km are suggested. If this is compared to the sedimentological and thermochronological evidence that the inversion in the north of the Rwenzori started about 2.5 to 2 Ma ago (Schneider et al., 2016), the slip rate on the Bwamba fault should be in the order of 1mm/year.

5. Conclusions

Previous studies of fault-related fluid migration are often concerned with fluid-rock interaction at the brittle-ductile transition, focusing on earthquake-cycling and mineralisation (Sibson, 1990, 2007; Cox, 1995). Consequently, there is limited information on fault behaviour in the upper crust, particularly in rift settings, where there is potential for fault zones to form hydrological links between basement and basin (Lueth et al., 2005; Hollis et al., 2017). Our study of a well-exposed basin-bounding rift fault reveals a complex record of fluid-rock interaction and gives important insights into fluid movements in an active rift zone in the shallow crust. Additionally, the BFZ represents an analogue for fluid migration at the margins of hydrocarbon-bearing rift basins (Logan et al., 2009), and those which host geothermal fluid circulation (Hollis et al., 2017). Our main conclusions are that:

- Permeability pathways in the BFZ were structurally controlled by fractures, brittle fabrics such as microfaults, cataclasite seams (some of which show Riedel, P-, R′, and Y-foliation geometries) and fractures. Permeability became restricted to fractures and some discrete cataclasite bands with an increase in the cataclasite matrix to survivor clast ratio. The development of the matrix indicates that cataclastic flow mechanisms were occurring, concurrent with brittle failure of cataclasites, and fragmentation of survivor clasts.
- An early fluid ingress event occurred, resulting K-feldspar and quartz veins in felsic fault rocks, and K-feldspar and carbonate veins in metabasic fault rocks. This was followed by a later event that precipitated Fe-oxide veins, and partial mineralisation of cataclasites by Fe-oxides and jarosite. Crystallisation temperatures are estimated to be ca. 150 °C.
- Two end-member models are established for fluid influx to the BFZ: the first involves co-seismic fluid influx, where dilating fractures and cataclasite seams draw in mineralising fluids; the second involves the formation of permeable pathways prior to fluid ingress, which occurs later during up fault migration of post-seismic

geothermal fluids.

- We propose a hydrological link developed between fluids in the Semliki Basin and the basement-hosted BFZ. Mobilisation of sulphur and iron from clastic and evaporitic rocks in the Semliki basin resulted in jarosite and Fe-oxide precipitation in the BFZ, as basin fluids were introduced to the fault zone due to its structural evolution. This seems a likely consequence of the change from a within basement normal fault to a rift basin margin fault. Such progressive evolution of fluid sources may be important for petroleum system behaviour in the Albertine Rift System and may be widely applicable to other rift-settings.

Acknowledgements

The authors would like Dr. Eric Salomon and Dr. Ake Fagereng for their insightful and detailed reviews. We thank Dr. Andreas Schuman and Kitam for their assistance during field work. We thank John Gilleece, Peter Chung and Les Hill for their assistance with sample preparation and photography. The work contained in this paper/publication/poster/presentation contains work conducted during a PhD study undertaken as part of the Natural Environment Research Council (NERC) Centre for Doctoral Training (CDT) in Oil & Gas [grant number NEM00578X/1]. It is sponsored by University of Glasgow via their NERC Scholarship whose support is gratefully acknowledged.

References

Abeinomugisha, D., 2010. Development of a petroleum system in a young rift basin prior to continental breakup : the albertine graben of the east African Rift system. In: AAPG International Conference and Exhibition, Calgary, Alberta, Canada, September, 12-15 (2010). AAPG Search and Discovery Article #10284.

Bahati, G., Pang, Z., Armannsson, H., Isabirye, E.M., Kato, V., 2005. Hydrology and reservoir characteristics of three geothermal systems in western Uganda. Geothermics 34 (4), 568–591.

Bauer, F.U., Glasmacher, U.A., Ring, U., Schumann, A., Nagudi, B., 2010. Thermal and exhumation history of the central Rwenzori Mountains, western rift of the east African Rift system, Uganda. Int. J. Earth Sci. 99 (7), 1575–1597.

Bauer, F.U., Karl, M., Glasmacher, U.A., Nagudi, B., Schumann, A., Mroszewski, L., 2012. The Rwenzori Mountains of western Uganda - aspects on the evolution of their remarkable morphology within the Albertine Rift. J. Afr. Earth Sci. 73 (74), 44–56.

Byerlee, J., 1993. Model for episodic flow of high-pressure water in fault zones before earthquakes. Geology 21 (4), 303–306.

Caine, J.S., Evans, J.P., Forster, C.B., 1996. Fault zone architecture and permeability structure. Geology 24 (11), 1025–1028.

Chester, F.M., Logan, J.M., 1986. Implications for mechanical properties of brittle faults from observations of the Punchbowl fault zone, California. Pure Appl. Geophys. PAGEOPH 124 (1–2), 79–106.

Chester, F.M., Friedman, M., Logan, J.M., 1985. Foliated cataclasites. Tectonophysics 111, 139–146.

Childs, C., Manzocchi, T., Walsh, J.J., Bonson, C.G., Nicol, A., Schopfer, M.P.J., 2009. A geometric model of fault zone and fault rock thickness variations. J. Struct. Geol. 31 (2), 117–127.

Cox, S.F., 1995. Faulting processes at high fluid pressures - an example of fault valve behavior from the wattle gully fault, Victoria, Australia. J. Geophys. Res.-Solid Earth 100 (B7), 12841–12859.

Ebinger, C.J., 1989. Tectonic development of the western branch of the East African rift system Tectonic development of the western branch of the East African rift system. Geol. Soc. Am. Bull. 101, 885–903.

Goren, L., Aharonov, E., Sparks, D., Toussaint, R., 2010. Pore pressure evolution in deforming granular material: a general formulation and the infinitely stiff approximation. J. Geophys. Res. 115 (B09216), 1–19.

Haines, S., Lynch, E., Mulch, A., Valley, J.W., van der Pluijm, B., 2016. Meteoric fluid infiltration in crustal-scale normal fault systems as indicated by d18O and d2 H geochemistry and 40Ar/39 Ar dating of neoformed clays in brittle fault rocks. Geol. Soc. Am. 8 (6), 587–600.

Harper, D.A., Longstaffe, F.J., Wadleigh, M.A., Mcnutt, R.H., 1995. Secondary K-feldspar at the precambrian paleozoic unconformity, southwestern Ontario. Can. J. Earth Sci. 32, 1432–1450.

Hodge, M., Fagereng, Å., Biggs, J., Mdala, H., 2018. Controls on early-rift geometry: new perspectives from the bilila-mtakataka fault, Malawi. Geophys. Res. Lett. 45 (9), 3896–3905.

Hofmann, C., Courtillot, V., Féraud, G., Rochette, P., Yirgu, G., Ketefo, E., Pik, R., 1997. Timing of the ethiopian flood basalt event and implications for plume birth and global change. Nature 389 (6653), 838–841.

Holdsworth, R.E., Stewart, M., Imber, J., Strachan, R.A., 2001. The structure and rheological evolution of reactivated continental fault zones: a review and case study. Geol. Soc. Lond. Spec. Publ. 184 (1), 115–137.

Holdsworth, R.E., van Diggelen, E.W.E., Spiers, C.J., de Bresser, J.H.P., Walker, R.J., Bowen, L., 2011. Fault rocks from the SAFOD core samples: implications for weakening at shallow depths along the San Andreas Fault, California. J. Struct. Geol. 33 (2), 132–144.

Hollis, C., Bastesen, E., Boyce, A., Corlett, H., Gawthorpe, R., Hirani, J., Rotevatn, A., Whitaker, F., 2017. Fault-controlled dolomitization in a rift basin. Geology 45 (3), 219–222.

Ikari, M.J., Niemeijer, A.R., Marone, C., 2011. The role of fault zone fabric and lithification state on frictional strength, constitutive behavior, and deformation microstructure. J. Geophys. Res. 116 (B08404), 1–25.

Japas, M.S., Urbina, N.E., Sruoga, P., Garro, J.M., Ibañes, O., 2016. A transient fault-valve mechanism operating in upper crustal level, Sierras Pampeanas, Argentina. J. Geodyn. 101, 142–154.

Kiconco, L., 2005. The Semliki Basin, Uganda: its Sedimentation History and Stratigraphy in Relation to Petroleum Accumulation. Unpublished Masters Thesis, University of Cape Town.

Koehn, D., Lindenfeld, M., Rümpker, G., Aanyu, K., Haines, S., Passchier, C.W., Sachau, T., 2010. Active transsection faults in rift transfer zones: evidence for complex stress fields and implications for crustal fragmentation processes in the western branch of the East African Rift. Int. J. Earth Sci. 99 (7), 1633–1642.

Kristensen, T.B., Rotevatn, A., Peacock, D.C.P., Henstra, G.A., Mmidtkandal, I., Grundvag, S., 2016. Structure and flow properties of syn-rift border faults: the interplay between fault damage and fault-related chemical alteration (Dombjerg Fault, Wollaston Forland, NE Greenland). J. Struct. Geol. 92, 99–115.

Last, R.J., Nyblade, A.A., Langston, C.A., Owens, T.J., 1997. Crustal Structure of the East African Plateau from Receiver Functions and Rayleigh Wave Phase Velocities.

Lawther, S., Dempster, T.J., Shipton, Z.K., Boyce, A., 2016. Effective crustal permeability controls fault evolution: an integrated structural, mineralogical and isotopic study in granitic gneiss, Monte Rosa, northern Italy. Tectonophysics 690, 160–173.

Lindenfeld, M., Rümpker, G., Batte, A., Schumann, A., 2012. Seismicity from february 2006 to september 2007 at the Rwenzori Mountains, East African rift: earthquake distribution, magnitudes and source mechanisms. Solid Earth 3 (2), 251–264.

Link, K., Koehn, D., Barth, M.G., Tiberindwa, J.V., Barifaijo, E., Aanyu, K., Foley, S.F., 2010. Continuous cratonic crust between the Congo and Tanzania blocks in western Uganda. Int. J. Earth Sci. 99 (7), 1559–1573.

Logan, P., Curd, S., Downie, B., Weston, J., Shaw, D., 2009. Exploration on the Frontier: towards an Understanding of the Albert Basin. pp. 1–6 10192.

Lueth, V.W., Rye, R.O., Peters, L., 2005. “Sour gas” hydrothermal jarosite: ancient to modern acid-sulfate mineralization in the southern Rio Grande Rift. Chem. Geol. 215 (1–4 SPEC. ISS), 339–360.

Mair, K., Frye, K.M., Marone, C., 2002. Influence of grain characteristics on the friction of granular shear zones. J. Geophys. Res. 107 (2219), 1–9.

Mitchell, T.M., Faulkner, D.R., 2012. Towards quantifying the matrix permeability of fault damage zones in low porosity rocks. Earth Planet Sci. Lett. 339 (340), 24–31.

Ochmann, N., Kraml, M., Babirye, P., Lindenfeld, M., 2010. Microearthquake survey at the Buranga geothermal prospect , western Uganda. In: Proceedings World Geothermal Congress, Bali, Indonesia, 25-29 April (2010), pp. 25–29.

Petit, J., 1987. Criteria for the sense of movement on fault surfaces in brittle rocks. J. Struct. Geol. 9 (5–6), 597–608.

Ring, U., 2008. Extreme uplift of the Rwenzori Mountains in the east African Rift, Uganda: structural framework and possible role of glaciations. Tectonics 27 (4), 1–19.

Roberts, E.M., Stevens, N.J., O'Connor, P.M., Dirks, P.H.G.M., Gottfried, M.D., Clyde, W.C., Hemming, S., 2012. Initiation of the western branch of the East African Rift coeval with the eastern branch. Nat. Geosci. 5 (4), 289–294.

Roller, S., Hornung, J., Hinderer, M., Ssemmanda, I., 2010. Middle Miocene to Pleistocene sedimentary record of rift evolution in the southern Albert Rift (Uganda). Int. J. Earth Sci. 99 (7), 1643–1661.

Sachau, T., Koehn, D., 2010. Faulting of the lithosphere during extension and related rift-flank uplift: a numerical study. Int. J. Earth Sci. 99 (7), 1619–1632.

Sachau, T., Koehn, D., Stamps, S.D., Lindenfeld, M., 2016. Fault kinematics and stress fields in the Rwenzori mountains, Uganda. Int. J. Earth Sci. 105 (6), 1729–1740.

Salomon, E., Koehn, D., Passchier, C., 2015. Brittle reactivation of ductile shear zones in NW Namibia in relation to South Atlantic Rifting. Tectonics 34 (1), 70–85.

Schneider, S., Hornung, J., Hinderer, M., 2016. Evolution of the western East African Rift system reflected in provenance changes of Miocene to pleistocene synrift sediments (Albertine Rift, Uganda). Sediment. Geol. 343, 190–205.

Sheldon, H.A., Ord, A., 2005. Evolution of porosity, permeability and fluid pressure in dilatant faults post-failure: implications for fluid flow and mineralization. Geofluids 5, 272–288.

Sibson, R.H., 1977. Fault rocks and fault mechanisms. J. Geol. Soc. 133 (3), 191–213.

Sibson, R.H., 1990. Conditions for fault-valve behaviour. Geol. Soc. Lond. Spec. Publ. 54 (1), 15–28.

Sibson, R.H., 2000. Fluid involvement in normal faulting. J. Geodyn. 29 (3–5), 469–499.

Sibson, R.H., 2007. An episode of fault-valve behaviour during compressional inversion ? — the 2004 M J 6 . 8 Mid-Niigata Prefecture, Japan, earthquake sequence. 257, 188–199.

Tenthorey, E., Cox, S.F., 2006. Cohesive strengthening of fault zones during the interseismic period: an experimental study. J. Geophys. Res. 111 (B09202), 1–14.

Trice, R., 2014. Basement exploration, West of Shetlands: progress in opening a new play on the UKCS. Geol. Soc. Lond. Spec. Publ. 397 (1), 81–939 105.

Upcott, N.M., Mukasa, R.K., Ebinger, C.J., 1996. Along-axis segmentation and isostasy in the Western rift, East Africa. J. Geophys. Res. 101 (B2), 3247–3268.

Wallner, H., Schmeling, H., 2010. Rift induced delamination of mantle lithosphere and crustal uplift: a new mechanism for explaining Rwenzori Mountains' extreme elevation? Int. J. Earth Sci. 99 (7), 1511–1524.

Wibberley, C.A.J., Shimamoto, T., 2002. Internal structure and permeability of major strike-slip fault zones: the median tectonic line in Mie prefecture, southwest Japan. J. Struct. Geol. 25 (1), 59–78.

Wölbern, I., Rümpker, G., Schumann, A., Muwanga, A., 2010. Crustal thinning beneath the Rwenzori region, Albertine rift, Uganda, from receiver-function analysis. Int. J. Earth Sci. 99 (7), 1545–1557.

Zhu, W., Wong, T., 1997. The transition from brittle faulting to cataclastic flow: permeability evolution. J. Geophys. Res. 102 (B2), 3027–3041.